Received: 11 March 2019 | Revised: 27 October 2019 | Accepted: 1 November 2019
DOI: 10.1002/pip.3224

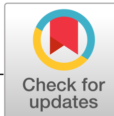

RESEARCH ARTICLE

WILEY PROGRESS IN PHOTOVOLTAICS

Electron radiation–induced degradation of GaAs solar cells with different architectures

Natasha Gruginskie[1] | Federica Cappelluti[2] | Gerard J. Bauhuis[1] | Peter Mulder[1] | Erik J. Haverkamp[1] | Elias Vlieg[1] | John J. Schermer[1]

[1]Institute for Molecules and Materials, Applied Materials Science, Radboud University, Heyendaalseweg 135, Nijmegen, 6525 AJ, The Netherlands

[2]Department of Electronics and Telecommunications, Politecnico di Torino, Corso Duca degli Abruzzi 24, Torino, 10129, Italy

Correspondence
Natasha Gruginskie, Institute for Molecules and Materials, Applied Materials Science Department, Radboud University, Heyendaalseweg 135, Nijmegen 6525 AJ, The Netherlands.
Email: n.gruginskie@science.ru.nl

Funding information
Conselho Nacional de Desenvolvimento Científico e Tecnológico, Grant/Award Number: 233259/2014-7; Horizon 2020 Framework Programme, Grant/Award Number: 687253 TFQD

Abstract

The effects of electron irradiation on the performance of GaAs solar cells with a range of architectures is studied. Solar cells with shallow and deep junction designs processed on the native wafer as well as into a thin-film were irradiated by 1-MeV electrons with fluence up to 1×10^{15} e^-/cm^2. The degradation of the cell performance due to irradiation was studied experimentally and theoretically using model simulations, and a coherent set of minority carriers' lifetime damage constants was derived. The solar cell performance degradation primarily depends on the junction depth and the thickness of the active layers, whereas the material damage shows to be insensitive to the cell architecture and fabrication steps. The modeling study has pointed out that besides the reduction of carriers lifetime, the electron irradiation strongly affects the quality of hetero-interfaces, an effect scarcely addressed in the literature. It is demonstrated that linear increase with the electron fluence of the surface recombination velocity at the front and rear hetero-interfaces of the solar cell accurately describes the degradation of the spectral response and of the dark current characteristic upon irradiation. A shallow junction solar cell processed into a thin-film device has the lowest sensitivity to electron radiation, showing an efficiency at the end of life equivalent to 82% of the beginning-of-life efficiency.

KEYWORDS
device modeling, electron radiation, GaAs solar cell, space application, thin-film solar cells

1 | INTRODUCTION

A standard space solar cell array consists of triple junction III-V cells on Ge wafer. These devices provide efficiencies well above 30%,[1] but they are rigid devices with relatively large weight. These cells are generally mounted on stabilizing panels consisting of an aluminum honeycomb structure sandwiched by carbon fiber reinforced polymer (CFRP) sheets, and a Ce-doped protective cover glass is applied on top of the system. The resulting array in these configurations can present specific mass around 2.6 kg/m^2.[2] In order to reduce the power-to-weight ratio of these systems, and therefore considerably reducing launching costs, the thickness of the Ge wafer used for epitaxial growth can be reduced,[3,4] which results in lighter yet rigid devices. By removing the growth substrate completely, the resultant solar cells consist of lightweight and flexible thin-film devices. These cells no longer require to be mounted on rigid panels for application, and when combined with new technologies for flexible front cover-glasses and mounting and deployment systems have the potential to reach specific mass of 0.6 kg/m^2.[2,5,6]

With some substrate removal techniques such as the epitaxial lift-off (ELO) process,[7-9] the expensive wafer can be applied to produce multiple cell structures,[10-12] further reducing the price of the solar cells.

By removing the Ge wafer, structures such as the tandem thin-film InGaP/GaAs solar cells appear to be promising for space solar arrays. The removal of the substrate also allows access to the rear contact, resulting in the development of new architectures.[13-15] Owing to the

This is an open access article under the terms of the Creative Commons Attribution License, which permits use, distribution and reproduction in any medium, provided the original work is properly cited.
© 2020 The Authors. Progress in Photovoltaics: Research and Applications published by John Wiley & Sons Ltd.

possibility of applying a back reflector, thin-film devices require smaller active layer thicknesses, further reducing costs related to both the weight and the growth of the epitaxial layers. The reflectivity of the rear mirror in high-quality materials has also been proven important to maximize photon recycling, which in turn increases the open circuit voltage and therefore the efficiency of the devices.[16-21]

In these structures, the bottom subcell consists of thin-film GaAs, which has demonstrated the highest conversion efficiency among all types of single junction solar cells.[1] Additionally to back contact design strategies,[22-24] the position of the junction in GaAs cells has been identified as an important parameter, showing that a device with the junction closer to the bottom of n-on-p cells allows for operation in the radiative recombination regime.[20,25,26] This type of cell, therefore, has a higher open circuit voltage and is preferred over the standard structure with a junction located closer to the front. But even though the deep junction design allows for better performance at the beginning-of-life, its resilience in the space environment is expected to be lower than that of the conventional shallow junction design.[27,28]

The most challenging aspects for solar cells in space are the exposure to particle irradiation and the temperature cycling. Because of the copper commonly applied as the flexible carrier for thin-film GaAs cells, degradation related to copper diffusion is a potential problem for devices with this architecture. It has been shown that the effects of copper-diffusion are temperature dependent, and for temperatures below 200°C, it does not reduce the cell performance in drastic degrees, provided the absence of damages induced by thermal stress, such as cracks or bends.[29]

The level of irradiation that cells would face throughout their entire lifetime in space depends on the type of mission. Based on the hypothesis that the permanent displacement damage produced by the incidence of charged particles is the main aspect that degrades the device performance in space, the mission equivalent damage from electrons, protons, ions, and neutrons of different energies can be averaged by a certain electron fluence.[30-33] Geostationary orbit missions (GEO) usually last for 15 years, and the damage created by the irradiation environment is equivalent to that obtained by a fluence of 1×10^{15} 1-MeV electrons/cm^2. For low earth orbit (LEO) missions, which last for approximate 10 years at a lower altitude, the equivalent fluences are five to 10 times lower.

The recombination centers formed in GaAs solar cells under irradiation have been studied in depth[30,31,33-36] and the implications of the junction position with lifetime degradation have been discussed.[27,28] It is generally understood that irradiation reduces the minority carriers' diffusion length, and therefore the average distance that these carriers have to travel before reaching the $p-n$ junction directly affect the cells resilience to the space environment. A systematic study of different architectures, however, has not yet been reported, and there is a lack of consistency between the previously reported minority carriers' lifetime degradation constants. Furthermore, in view of the current trend of developing thin and ultra-thin radiation-hard solar cells,[14] knowledge of the possible impact of irradiation on emitter-window and base-BSF hetero-interfaces surface recombination velocities is becoming increasingly important. For silicon cells, Imaizumi et al already suggested, based on EQE analysis, that irradiation has increased the surface recombination velocity.[37]

In the current study, the possible influence of electron irradiation on hetero-interfaces of GaAs solar cells is systematically investigated. For this purpose, GaAs cells with different junction depths with respect to the hetero-interfaces, both on their native substrates and processed into genuine thin-film devices, are subjected to 1-MeV electron radiation. A consistent model is applied in order to simulate the experimental results from all the different cell geometries simultaneously, and a coherent set of minority carriers' lifetime damage constants is derived. At the same time, the actual relations between the electron fluence and resulting surface recombination velocities of the front and rear hetero-interfaces of the cells are determined.

2 | METHODS

2.1 | Experimental details

Solar cells with different structures were subjected to a total electron fluence of 1×10^{15} e$^-$/cm^2 of 1-MeV radiation, which corresponds to a 15-year GEO mission.[32] The irradiation was performed at the Reactor Institute Delft (RID) of the Delft University of Technology, using a van der Graaf accelerator with an electron flux of 5×10^{11} e$^-$/cm^{2}s. The available structures for this study consisted of two substrate-based (SB) and three thin-film (TF) GaAs solar cells, with either a thin n-doped emitter and a thick p-doped base, here called a shallow junction (SJ) geometry, or a thick n-doped emitter and a thin p-doped base, here called a deep junction (DJ) geometry, as depicted in Figure 1.

The thickness and doping levels of the layers, as obtained by MOCVD growth on 2-inch (100) GaAs wafers 2° off to (110) orientation, are summarized in Table 1. It is important to notice that the SB-DJ solar cells have a heterojunction, meaning that an InGaP layer functions both as base and as back surface field (BSF). Because we expect the thickness to have an impact on the degradation,[34] most of the structures have comparable GaAs thickness, and one of the thin-film cell structures has a significantly thinner (1400 nm) active layer, which will be referenced as TF-DJ$_{1400nm}$.

The cells all have e-beam evaporated metal contacts and thermally evaporated MgF_2/ZnS ARC coatings. Their cell areas were defined by a MESA etch using an ammonia:hydrogen peroxide solution for the GaAs layers and either HCl 37% or a HBr:Br_2:H_2O solution for the phosphide layers. The top n-GaAs contact layer between the grid fingers was removed also using an ammonia:hydrogen peroxide solution. The substrate-based solar cells measure 1×1 cm^2 and have a frontal metal grid consisting of 100-nm-thick Au and 6000-nm Cu, covering 1.2% of the total area. After processing, the substrate-based cells were diced and individually mounted on a chip carrier (see Figure 2A). The thin-film cells measure 0.5×0.5 cm^2 and have 200-nm-thick Au front contact that covers 16.6% of the cell area. The substrates were simply removed by etching with an aqueous citric acid and hydrogen peroxide solution. Subsequently, a 200-nm-thick full Au contact/mirror was evaporated onto the rear side of the cell and the structures were mounted on a copper foil that acts as a conductive foreign carrier. The foils consisting of multiple cells and several dedicated structures without grid for EQE analysis were glued as a whole on a glass handling carrier (see Figure 2B).

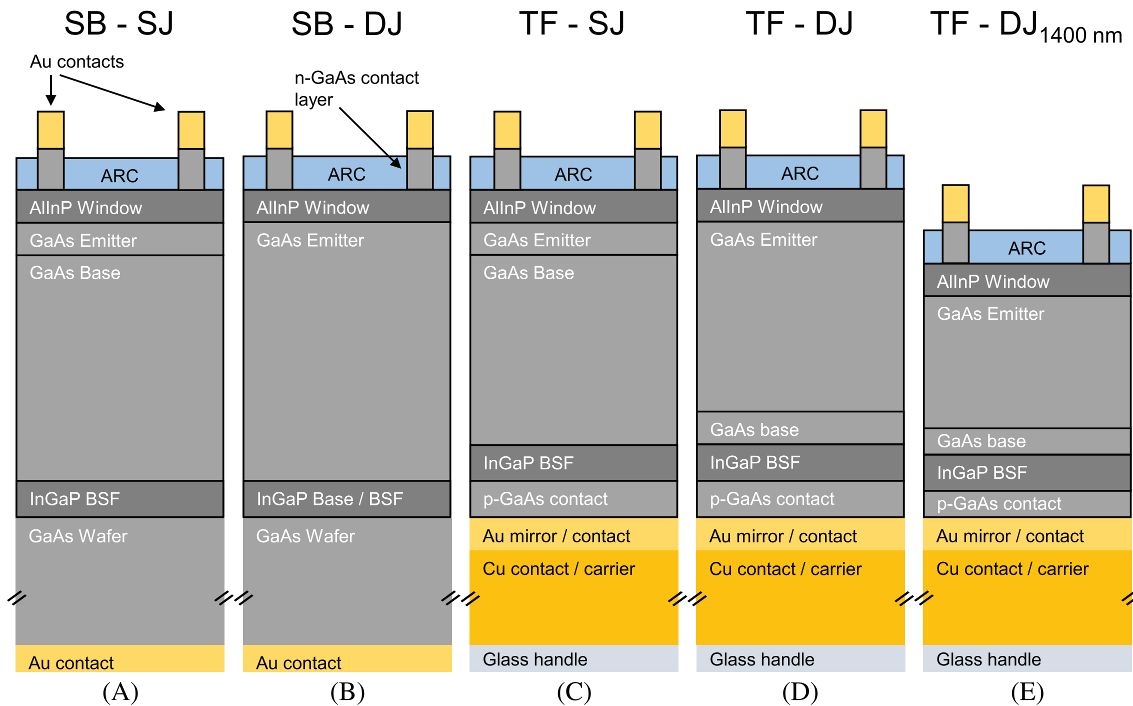

FIGURE 1 Device schematic of the five different GaAs cell geometries under study: A, substrate based shallow junction, B, substrate based deep junction, C, thin-film shallow junction, D, thin-film deep junction, and E, thinner thin-film deep junction [Colour figure can be viewed at wileyonlinelibrary.com]

TABLE 1 Summary of solar cell structures used in this study

Solar Cell Reference	Solar Cell Architecture	Emitter Thickness, nm	Base Thickness, nm	Emitter n-doping, cm^{-3}	Base p-doping [cm^{-3}]
SB-SJ	Subst. based	100	2100	3×10^{18}	3×10^{16}
SB-DJ	Subst. based	2200	100	5×10^{16}	5×10^{17}
TF-SJ	Thin-film	75	2000	3×10^{18}	3×10^{16}
TF-DJ	Thin-film	2000	75	5×10^{16}	1×10^{18}
$TF\text{-}DJ_{1400nm}$	Thin-film	1320	80	5×10^{16}	1×10^{18}

For each configuration, three to nine individual solar cells were irradiated and characterized. The irradiation was interrupted five times in the interval between 1×10^{13} and 1×10^{15} e^-/cm^2 to allow for intermediate on-site $J-V$ measurements under AM1.5G conditions, with a constant intensity in the range of 990 to 1010 W/m^2 and at a temperature of 25°C ±2.5°C. For this purpose, a mobile set-up consisting of a Keithley 2401 multimeter with a portable solar simulator was used while ReRa Tracer3 was applied for data acquisition. By measuring the short current density of an NREL calibrated reference cell before each measurement series, the measured currents of the cells could be scaled to the corresponding values under exactly 1000 W/m^2. With this approach, mutual comparison between different cell geometries can be identified with an accuracy of ±2 mV in V_{oc}, ±0.06 mA/cm^2 in J_{sc}, and ±0.003 in FF. The on-site characterization allowed for a minimal interval in between measurements, which dependent on the irradiation time ranged from 10 to 60 minutes.

The external quantum efficiency (EQE) and dark $J-V$ characteristics were measured at the Radboud University before and after all irradiation experiments performed at the RID. The EQE measurements were obtained with a ReRa SpeQuest Quantum Efficiency system, and dark $J-V$ characteristics were obtained using a Keithley 2601B source meter and a heating/cooling water thermostat with a Pt100 temperature sensor to keep the solar cells at a temperature of 25°C. Because the series resistance bends the dark curve downwards at higher voltages, a curve composed of short-circuit current (J_{sc}) and open circuit voltage (V_{oc}) values measured under different light intensities represents the ideal diode dark characteristics, as the series resistance is excluded under these conditions.[38] From each configuration, one cell was removed before subjecting the cells to the last irradiation dose in order to obtain EQE and dark $J-V$ curves of cells subjected to intermediate irradiation levels, with the exception of the TF-SJ and $TF\text{-}DJ_{1400}$.

2.2 | Device model

The solar cells subjected to 1-MeV irradiation have been analyzed based on the 1D analytical Hovel model[39] and its extended version for thin-film solar cells with back-side reflector.[40] The model formulation is rather general and well suited to describe different solar cell designs provided that material and geometry parameters are changed accordingly. A schematic depiction of the modeled structure and corresponding variables used in this study are shown in Figure 3, where X_E and X_B denote the thickness of the emitter and base layers, respectively, and W denotes the width of the depleted region across the junction.

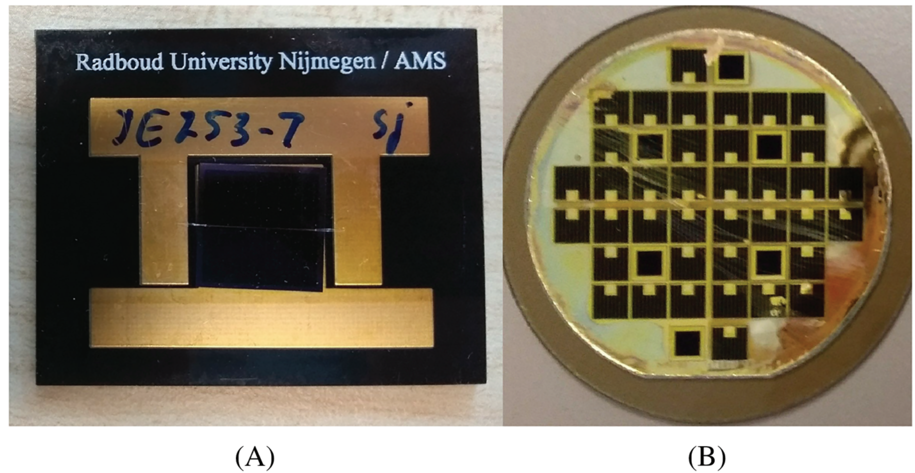

FIGURE 2 Photograph of A, an individual 1 × 1 cm^2 substrate-based solar cell mounted on a PCB board and B, a set of multiple 0.5 × 0.5 cm^2 thin-film solar cells on a copper foil, mounted on a glass plate for safe handling. The latter also shows a darkening of the glass plate after irradiation [Colour figure can be viewed at wileyonlinelibrary.com]

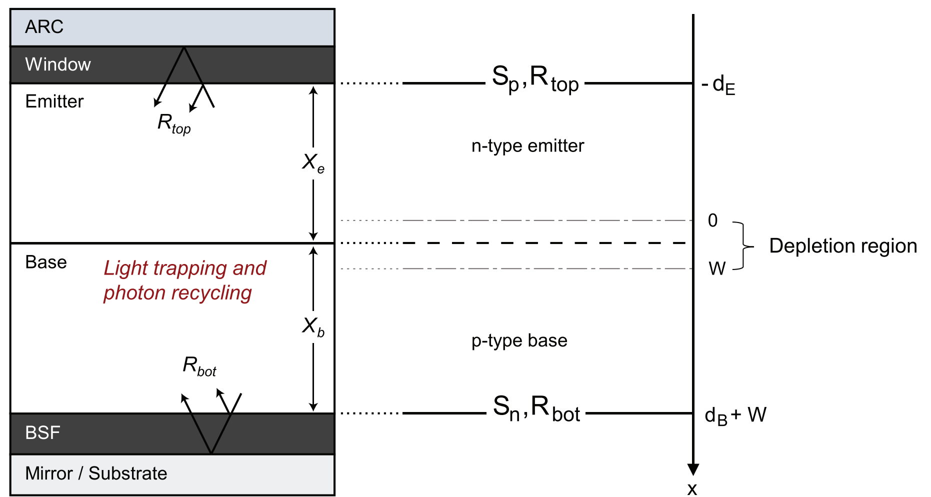

FIGURE 3 Schematic representation of the modeled solar cell structure with the 1D cut-line and parameters definition used in the analytical model (adapted from Lumb et al[40]) [Colour figure can be viewed at wileyonlinelibrary.com]

Under monochromatic illumination, and assuming negligible electrical field and constant material parameters, carrier transport in the quasi neutral regions is modeled by the diffusion equation of minority carriers, including the distributed optical generation term. The effect of window and back surface field layers is phenomenologically described by the interface recombination velocity of *p*-type minority carriers at the emitter-window interface (S_p) and of *n*-type minority carriers at the base-BSF interface (S_n), which set the boundary conditions for the diffusion equations in the emitter and base QNRs. At the edge of the depletion-QNR regions, the voltage-dependent excess minority carrier density is calculated through the exponential junction law. Such formulation yields a closed form analytical expression for the optical- and voltage-dependent current contributions associated to the two QNRs. The total spectral photocurrent and the associated EQE results as the sum of the emitter and base QNR contributions and the contribution from the depletion region (where collection efficiency is assumed to be unitary) computed under monochromatic excitation and short-circuit condition. The short circuit current density is calculated by integrating the specific illumination spectrum weighted by the EQE over the wavelength. Concerning the optical generation rate, the distribution of the optical field is calculated based on multiple reflections between the window-emitter interface and the base-BSF interface, characterized by the top reflectance (R_{top}) and by the bottom reflectance (R_{bot}), respectively. The wavelength dependent R_{top} and R_{bot} are derived from 1D electromagnetic simulations for coherent multilayers, using material optical data taken from the literature[41] for GaAs, and from ellipsometry measurements for the other materials. Further model details and the resulting analytical expressions can be found in previous works.[39,40]

The transport and collection of minority carriers are determined by the diffusion length, given by $L_\alpha = \sqrt{D_\alpha \tau_\alpha}$, where the subscript α identifies electrons (*n*) in the base and holes (*p*) in the emitter. D_α is the diffusion coefficient and τ_α is the minority carrier lifetime. The doping dependent parameters D_n and D_p were defined according to the model described by Sotoodeh et al.,[42] and τ_α is calculated under low injection conditions considering both radiative and defect mediated non-radiative recombination as

$$\frac{1}{\tau_\alpha} = \frac{1 - f_{PR}}{\tau_{\alpha,rad}} + \frac{1}{\tau_{\alpha,SRH}}, \tag{1}$$

where the radiative lifetime is given as $\tau_{\alpha,rad} = 1/BN_{AB(DE)}$, B being the microscopic radiative recombination rate of the semiconductor, and N_{AB}, N_{DE} the acceptor and donor doping density in the base and emitter. For the sake of thermodynamic consistency, the coefficient B is calculated by integrating the spontaneous emission rate associated with the GaAs absorption profile used in the CPS and is found to be 6.22×10^{-10} cm^3/s. Photon recycling is modeled through the photon recycling factor f_{PR}, calculated according to the model reported by Steiner et al.[19] For the solar cells in this study the calculated f_{PR} ranges from approx-

imately 0.78 for the substrate based cells to 0.93 for the thin-film devices. Finally, $\tau_{\alpha,SRH}$ characterizes the non-radiative recombination lifetime. At the microscopic level, $\tau_{\alpha,SRH}$ results from electron-hole recombination and generation events through defect states whose rates can be modeled according to the classical Shockley-Read-Hall theory. Multiple defects can be taken into account, provided that they can be considered independent, characterized by their own density, energy and capture time constants. Under the assumption of low-level injection, exploited in this work, this yields a constant effective lifetime, $\tau_{\alpha,SRH}$, independent of the injection level and dominated by the defect state with higher rates, i.e. those generally located close to mid-gap.[43] Therefore, in the present work, $\tau_{\alpha,SRH}$ was used as a fitting parameter and no a priori hypothesis was done on the nature and characteristics of the defect levels.

After de-embedding the possible influence of the parasitic series and shunt resistances, the dark $J-V$ characteristic (J_{dark}) of the solar cell can be modeled by two diodes in parallel[25]:

$$J_{dark} = J_{01}\left(e^{\frac{qV}{kT}} - 1\right) + J_{02}\left(e^{\frac{qV}{2kT}} - 1\right), \quad (2)$$

where J_{01} and J_{02} are the reverse saturation current densities of the $1kT$ and $2kT$ components, respectively, and q, k, and T the electron charge, Boltzmann constant and temperature. The ratio between the two components of the dark current is voltage dependent, with non-radiative recombination in the perimeter of the cell and in the space-charge region dominating at low voltages (the $2kT$ region) and recombination in the quasi-neutral regions (QNR) dominating at higher voltages (the $1kT$ region). According to the junction diffusion theory, J_{01} arises from the bulk and interface recombination of minority carriers in the base and emitter QNR regions [39] and is given by

$$J_{01} = J_{01,E} + J_{01,B}, \quad (3a)$$

with each component given by

$$J_{01,E} = \frac{qD_p n_{i,E}^2}{L_p N_{DE}} \times \frac{\sinh\frac{d_E}{L_p} + \frac{S_p L_p}{D_p}\cosh\frac{d_E}{L_p}}{\cosh\frac{d_E}{L_p} + \frac{S_p L_p}{D_p}\sinh\frac{d_E}{L_p}}, \quad (3b)$$

and

$$J_{01,B} = \frac{qD_n n_{i,B}^2}{L_n N_A} \times \frac{\sinh\frac{d_B}{L_n} + \frac{S_n L_n}{D_n}\cosh\frac{d_B}{L_n}}{\cosh\frac{d_B}{L_n} + \frac{S_n L_n}{D_n}\sinh\frac{d_B}{L_n}}, \quad (3c)$$

where d_B and d_E are the thickness of the QNR of the base and emitter with intrinsic carrier density $n_{i,B}^2$ and $n_{i,E}^2$, respectively. The intrinsic carrier density is computed taking into account the bandgap narrowing effect in the highly doped regions. In particular, the bandgap narrowing significantly affects the QNR recombination current in the highly doped base and emitter layer of the DJ and SJ cells, respectively. We have assumed bandgap shrinkage $\Delta E_g \approx 2\times10^{-11}N_{AB}^{1/2}$ eV for p-type GaAs[44] and $\Delta E_g \approx 2\times10^{-8}N_{DE}^{1/3}$ for n-type GaAs.[45] The J_{02} dark current component involves non radiative recombination mechanisms in the space charge region that can usually be modeled according to the Shockley-Read-Hall theory,[40,46] with analytical or semi-analytical formulations available under the assumption of a single mid-gap defect level[46] and for the more realistic case of multiple trap levels.[33]

TABLE 2 Measured and simulated BOL values for J_{sc} and V_{oc} of the different solar cell geometries

Solar Cell	J_{sc}, mA/cm^2		V_{oc}, V	
Geometry	Measured	Simulated	Measured	Simulated
SB-SJ	28.1	28.1	1.053	1.053
SB-DJ	27.3	28.3	1.070	1.058
TF-SJ	24.5	24.5	0.996	0.996
TF-DJ	24.3	25.1	1.043	1.042
TF-DJ$_{1400nm}$	24.3	24.1	1.035	1.035

3 | RESULTS AND DISCUSSION

3.1 | Overview of the performance at BOL and upon irradiation

The average photovoltaic cell parameters measured at BOL for the different device architectures are reported in Table 2 and compared with the simulated values. When corrected to the active area, the solar cells present efficiencies close to 25% under AM1.5G, and close to 21.5% under AM0 (1367 W/m^2 at 28°C). The produced thin-film solar cells mounted on a metal foil present a specific power above 1200 W/kg, and when combined with light weight mounting systems and flexible protective coatings for space application they show the potential to reach a module specific power above 400 W/kg. [2]

In order to identify the four model parameters S_p, S_n, τ_p, and τ_n before and after irradiation, EQE spectra, illuminated and dark $J-V$ parameters at BOL and upon irradiation were considered. The parameter extraction procedure emphasizes the fitting of the average photovoltaic parameters ensuring at the same time a good correlation with the measured EQE spectra and dark $J-V$ of single representative samples. The modeled BOL values of both the short circuit current (J_{sc}) and the open-circuit voltage (V_{oc}) reported in Table 2 are very representative of the measured values and indicate a good quality of the epitaxial layers. The measured V_{oc} values are all within 1% of the simulated values, and a slightly larger variation is seen for the J_{sc}, probably due to a non-perfect deposition of the ARC layers, which can directly affect the experimentally obtained current. Note that the J_{sc} values of the TF cells are significantly lower than that of the SB cells because their grid coverage is much higher. When J_{sc} is corrected for the effective exposed area, the values are comparable.

The effect that the electron irradiation has on the illuminated $J-V$ parameters is expressed in terms of the remaining factor with respect to the BOL values, defined as $Parameter/Parameter_{BOL}$. The average experimentally determined remaining factors from J_{sc} and V_{oc} are shown in Figure 4A,B, respectively. It is clear that the J_{sc} of both thin-film and substrate based devices with a SJ geometry show relatively small sensitivity to electron radiation damage, with EOL remaining factors above 90%. On the other hand, the cells with the DJ geometry are severely affected by the irradiation, showing EOL J_{sc} remaining factors of approximately 15% for substrate based cells, 25% for the thin-film cells and 55% for the thinner thin-film sample. The V_{oc} of the solar cells is in general less sensitive to electron radiation, presenting EOL remaining factors above 75% for all samples and above 85% for all cells with the exception of the SB - DJ cells. For fluences

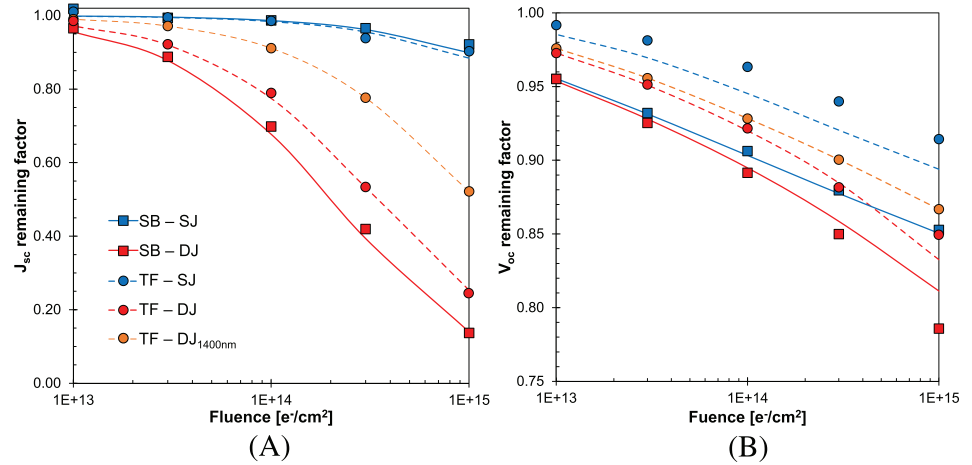

FIGURE 4 Remaining factors of A, the J_{sc} and B, the V_{oc} of the solar cells subjected to different fluences of 1-MeV electron radiation. The markers represent the average of the measured values and the lines are the best fit of the CPS model to the experiments [Colour figure can be viewed at wileyonlinelibrary.com]

up to 3×10^{14} e$^-$/cm^2, usually associated with LEO missions,[32] both SJ and DJ cells in the thin-film architecture clearly show less degradation of V_{oc} than the substrate-based cells.

The lines in Figure 4 represent the CPS model fit to the experimental remaining factors. The simulated J_{sc} values agree closely with the measurements, while there is a slightly larger deviation (maximum of 2% absolute) between the simulated and measured V_{oc} remaining factor values. This can be related to the fact that illuminated $J-V$ measurements were performed with a portable solar simulator that has a less precise temperature control (with variations from 25°C up to ±2.5°C), which will most strongly affect the V_{oc}.

The modeled efficiency remaining factors match the measured values within 5% relative, as shown in Table 3. The remaining efficiencies are clearly higher for SJ than for DJ cells, and are higher for both geometries in a thin-film design than when they are substrate based, since the thin-film devices are thinner. The thinner DJ sample presents an intermediate EOL efficiency remaining factor, indicating a strong influence of the solar cell thickness on the performance under electron radiation.

Table 4 summarizes the BOL and EOL values for the minority carriers lifetime, the diffusion length, and the surface recombination velocity at the window and BSF interfaces, as derived from the best fit of the CPS model to the average experimental BOL and the average remaining factors *vs.* fluence. As discussed in the following, the performance at BOL is well reproduced by the CPS model assuming the nominal minority carrier lifetimes calculated from Equation (1) and accounting - whenever needed - for an imperfect passivation at the window and BSF interfaces. Following this approach specifically

TABLE 3 Efficiency remaining factors of the solar cells at at EOL

Solar Cell	η Remaining Factors:	
Geometry	Measured	Simulated
SB-SJ	0.79	0.75
SB-DJ	0.10	0.10
TF-SJ	0.82	0.78
TF-DJ	0.19	0.20
TF-DJ$_{1400nm}$	0.45	0.44

clarifies that the V_{oc} of the thin-film cells turns out to be limited by the surface recombination velocity at the base-BSF interface (S_n). Upon exposure to radiation, the minority carriers lifetime reduces (most likely due to radiation displacement defects[30-34]). Furthermore, in all solar cell structures a degradation of the emitter-window (GaAs/AlInP) and base-BSF (GaAs/InGaP) hetero-interfaces quality is identified, characterized by an increase in the surface recombination velocity.

3.2 | Analysis at BOL

The window and BSF layers are high bandgap materials that have the function of repelling minority carriers away from the surfaces of the cell, which are areas of high SRH recombination probabilities. Based on previous results of cells grown under the same conditions as in this study,[25] a good quality in the growth of the hetero-interfaces GaAs/AlInP and GaAs/InGaP is assumed. Consequently, an effective surface passivation by the window and BSF layers is expected, and therefore S_p and S_n are initially considered to be negligible.

The emitter and base lifetimes were estimated at beginning of life (BOL) from Equation (1), with SRH lifetimes given by the empirical model of Lumb et al.[20] Under these assumptions, it turns out that at BOL the carrier lifetimes are dominated by radiative recombination in all the layers, except for the highly doped base of the deep-junction cells, where SRH and radiative recombination lifetimes are similar.

For layers with similar doping levels, such as the emitter in the DJ cells and the base in the SJ cells, L_p is smaller than L_n because the hole mobility is markedly lower than the electron mobility. The higher lifetimes observed in the TF cells with respect to the corresponding SB devices are explained by the higher photon recycling factor, and therefore higher radiative lifetime, of the TF cells. For a high collection efficiency the devices should present $d_E \ll L_p$ and $d_B \ll L_n$, and this is the case for all the structures, as demonstrated by the high EQE at BOL seen in Figures 5 and 6 for the SJ and DJ cells, respectively. Hence, the calculated lifetimes used in the model, which are approximations for high quality materials, are justified by the high BOL efficiency of the studied devices, and in fact provide a very good fitting of the measured EQE.

In the DJ solar cells, the base is responsible for the absorption of approximately 0.2% of the photons only,[25] and therefore the EQE is

TABLE 4 Minority carrier lifetimes, diffusion lengths and surface recombination velocities for each solar cell configuration at BOL and EOL, as deduced from the best fits of the model to the average measured photovoltaic parameters at BOL and upon irradiation

Solar Cell Geometry	BOL						EOL					
	τ_p (ns)	L_p (µm)	S_p (cm/s)	τ_n (ns)	L_n (µm)	S_n (cm/s)	τ_p (ns)	L_p (µm)	S_p (cm/s)	τ_n (ns)	L_n (µm)	S_n (cm/s)
SB-SJ	1.90	0.81	<100	133	43.6	360	0.71	0.50	1.7×10^4	0.19	1.65	(360)
SB-DJ	138	10.4	1.3×10^3	8.5	8.4	<100	0.57	0.67	3.6×10^4	(0.19)	(1.13)	1.3×10^7
TF-SJ	3.8	1.14	2.0×10^4	203	54.0	1.2×10^4	0.88	0.55	5.4×10^4	0.19	1.65	(1.2×10^4)
TF-DJ	346	16.5	<100	6.8	6.9	2.6×10^4	1.14	0.95	6.7×10^4	(0.19)	(2.8)	4.6×10^6
TF-DJ$_{1400nm}$	346	16.5	3×10^3	6.8	6.9	1.2×10^4	1.14	0.95	4.9×10^4	(0.19)	(1.13)	6.5×10^6

Note. At BOL, the values of $\tau_n(p)$ and $L_n(p)$ are the nominal ones and only S_n and S_p are used as fitting parameters. At EOL, both lifetime and surface recombination velocity are used as fitting parameters. The values presented in parentheses may be affected by a large error.

dominated by the emitter collection efficiency, ie, by S_p and τ_p. From the EQE fitting, τ_p is found consistent with the expected theoretical value for all the three DJ samples, while a non negligible S_p explains the slightly lower EQE of the thinner DJ cell. On the other hand, the values of τ_n and S_n do not significantly affect the collection efficiency in the thin base and cannot be extracted from the EQE spectra. Some insight on the base parameters and on the V_{oc} degradation can be instead derived from the measured dark $J-V$ characteristics reported in Figure 7, and in particular from the analysis of the 1kT dark current component. The J_{01} and J_{02} values extracted from fitting the two-diode model (Equation 2) to the measured dark $J-V$ curves of the different cells are summarized in Table 5.

Figure 8 shows the calculated values for $J_{01,B}$ and $J_{01,E}$ as a function of the minority carriers lifetime and for values of S_p and S_n varying logarithmically from 10^0 to 10^7 cm/s, for cells with a GaAs emitter-base homo-junction and layers thickness of the actual TF - SJ and DJ designs. The effect of the interface recombination velocity on J_{01} increases with the probability of carriers to reach the hetero-interfaces, being almost irrelevant in case of short lifetimes and more pronounced for thin layers. In the limit of thick QNR ($L_{p(n)} \ll d_{E(B)}$), J_{01} is dominated by bulk recombination and Equations (3a) to (3c) reduce to the classical Shockley equation:

$$J_{01} = J_{01,E} + J_{01,B} = \frac{qD_p n_{i,E}^2}{L_p N_{DE}} + \frac{qD_n n_{i,B}^2}{L_n N_{AB}}, \quad (4)$$

whereas for thin QNR ($L_{p(n)} \gg d_{E(B)}$), J_{01} is dominated by surface recombination and Equations (3a) to (3c) reduce to

$$J_{01} = J_{01,E} + J_{01,B} = \frac{qn_{i,E}^2 D_p}{N_{DE}} \frac{S_p}{D_p + S_p d_E} + \frac{qn_{i,B}^2 D_n}{N_{AB}} \frac{S_n}{D_n + S_n d_B}. \quad (5)$$

The SJ design presents a strongly asymmetric doping ($N_{DE}/N_{AB} = 100$), and therefore, the base dark current component tends to be highly dominant (Figure 8A). On the other hand, in the DJ design ($N_{AB}/N_{DE} = 20$) the emitter and base dark current components provide more similar contributions (Figure 8B).

Using the values of τ_p and S_p deduced from the EQE measurements of the DJ solar cells, the $J_{01,E}$ component (Equation 3b) is about one-fifth of the J_{01} value extracted from the two-diode fitting (Equation 2, Table 5). This indicates a significant contribution to J_{01} from the base layer. In fact, as can be verified in Figure 8B, matching the measured value requires the assumption of a very short lifetime of electrons in the base ($\tau_n \approx 0.3$ ns if $S_n \leq 10^3$ cm/s) or, the more realistic alternative adopted here, a non-negligible surface recombination S_n on the order of 3×10^4 cm/s if one considers for τ_n the nominal BOL value of a few ns.

It is worth noticing that in the case of the SB-DJ cells, which have an InGaP ($E_g \approx 1.8$ eV) base layer, the dark current contribution from the base QNR is expected to be negligible with respect to that of the emitter QNR, regardless of the electron lifetime and surface recombination velocity. On the other hand, the measured data indicate, already at BOL, an unexpected high recombination

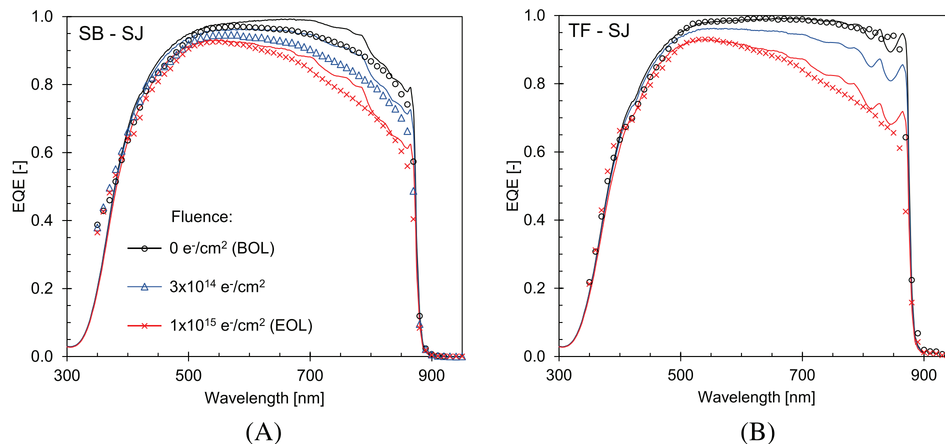

FIGURE 5 External quantum efficiency of A, substrate based and B, thin-film solar cells with a shallow junction geometry under different levels of irradiation. The markers represent the measured data and the lines the simulation results [Colour figure can be viewed at wileyonlinelibrary.com]

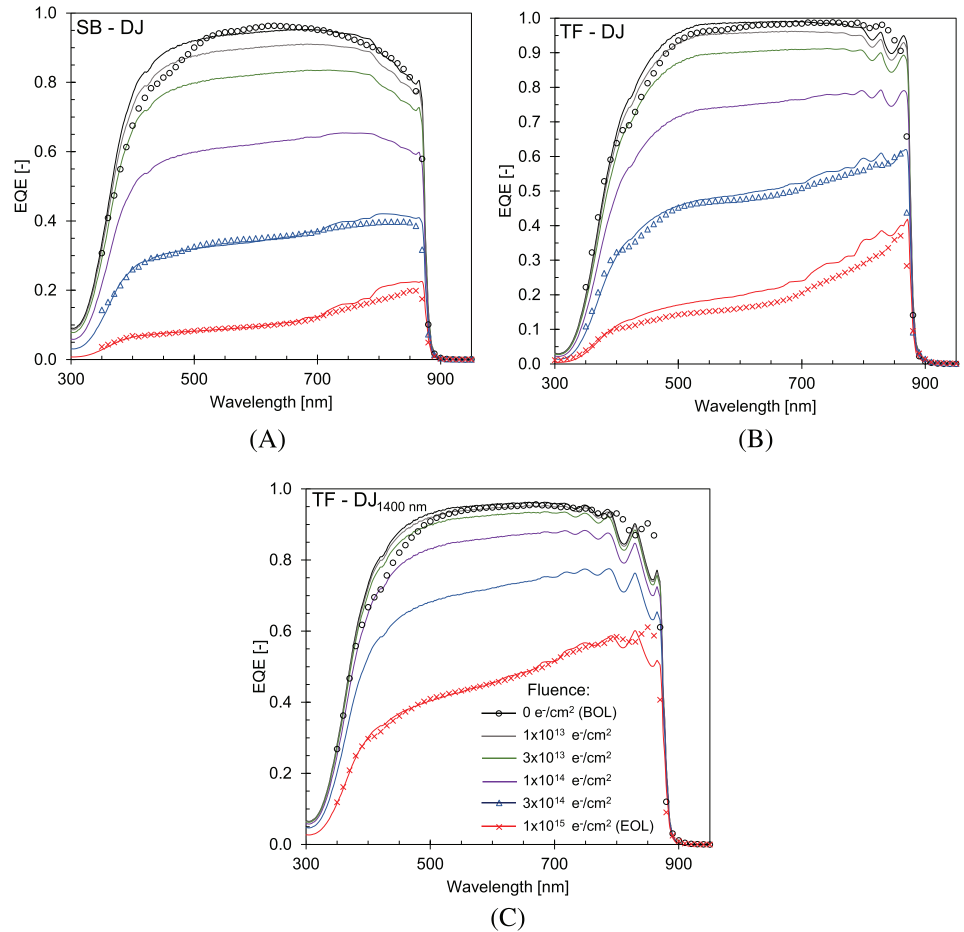

FIGURE 6 External quantum efficiency of A, the substrate based, B, the thin-film, and C, the thinner thin-film solar cells with a deep junction geometry under different levels of irradiation. The markers represent the measured data and the lines the simulation results [Colour figure can be viewed at wileyonlinelibrary.com]

current with unitary ideality factor. In the context of this work, such high current has been accounted for by modeling the InGaP base layer with a fictitiously high intrinsic carrier density, of the same order of that of GaAs. In this respect, further investigation on the GaAs-InGaP emitter-base heterojunction and the associated interface recombination mechanisms is needed.

Concerning the SJ cells, both the QNRs and the depletion region give substantial contribution to the spectral photocurrent, which shows a large resilience to low carrier lifetimes and high interface recombination velocities. In particular, the EQE in the region around 650 nm is hardly affected by τ_α and S_α, being sustained by the depletion region. Based on the applied theoretical emitter minority carrier lifetimes reported in Table 4, there is a good match between the modeled and experimental EQE in the short wavelength range. On the other hand, however, solely based on EQE, it is not possible to accurately determine τ_n and S_n. As in the DJ case, this can be resolved to some extent by studying the J_{01} component around V_{oc}, which is dominated by recombination in the base QNR. The SB - SJ cells show a low J_{01} ($\approx 4\times10^{-20}$ A/cm^2), coherently with the high theoretical τ_n value of about 100 ns and a low S_n on the order of few hundreds of cm/s. In contrast, the TF - SJ cells show a significantly higher J_{01} ($\approx 3\times10^{-19}$ A/cm^2) that is attributed to an S_n comparatively higher than that of the SB structure, as also observed for the DJ cells.

Overall, it turns out that in both DJ and SJ geometries τ_p and S_p are the predominant factors affecting the EQE at BOL, while τ_n and S_n mainly influence the V_{oc} through the recombination current in the p-type QNR region.

3.3 | Analysis of bulk and interface radiation damage

In order to simulate the cell performance after intermediate electron irradiation doses, the decrease of the SRH lifetime $\tau_{\alpha,SRH}$ with radiation is modeled as

$$\frac{1}{\tau_{\alpha,SRH}} = \frac{1}{\tau_{\alpha,SRH0}} + K_{\tau_\alpha}\phi, \quad (6)$$

TABLE 5 Saturation current densities J_{01} and J_{02} deduced from the dark $J-V$ curves of the various cell geometries using the two-diode model

Solar Cell	0 e$^-$/cm^2 (BOL)		3×10^{14} e$^-$/cm^2		1×10^{15} e$^-$/cm^2 (EOL)	
Geometry	J_{01}, $\frac{A}{cm^2}$	J_{02}, $\frac{A}{cm^2}$	J_{01}, $\frac{A}{cm^2}$	J_{02}, $\frac{A}{cm^2}$	J_{01}, $\frac{A}{cm^2}$	J_{02}, $\frac{A}{cm^2}$
SB-SJ	4.0×10^{-20}	3.0×10^{-12}	8.0×10^{-18}	2.5×10^{-11}	2.3×10^{-17}	4.2×10^{-11}
SB-DJ	3.5×10^{-20}	1.1×10^{-12}	6.9×10^{-18}	8.8×10^{-12}	2.7×10^{-17}	2.1×10^{-11}
TF-SJ	3.0×10^{-19}	1.2×10^{-11}	–	–	1.2×10^{-17}	2.6×10^{-11}
TF-DJ	7.0×10^{-20}	4.0×10^{-12}	5.0×10^{-18}	3.8×10^{-11}	2.6×10^{-17}	5.3×10^{-11}
TF-DJ$_{1400nm}$	–	–	–	–	2.0×10^{-17}	6.4×10^{-11}

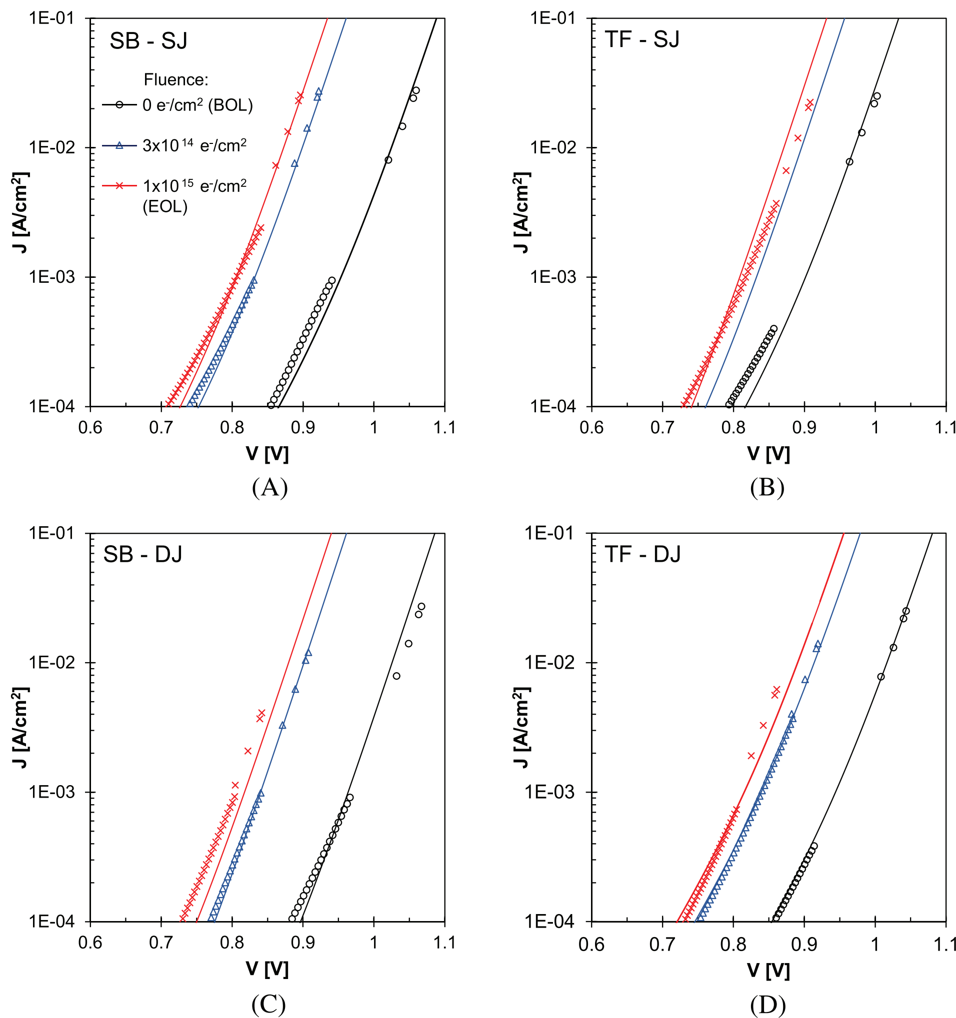

FIGURE 7 Dark current-voltage characteristics of A, the substrate based shallow junction, B, the thin-film shallow junction, C, the substrate based deep junction, and D, the thin-film deep junction solar cells after different levels of 1-MeV electron irradiation. Note that the upper four data points were obtained using J_{sc} - V_{oc} pairs at different illumination intensities. The markers represent the measured data and the solid lines the two-diode model with J_{01} calculated from the CPS model [Colour figure can be viewed at wileyonlinelibrary.com]

where $\tau_{\alpha,SRH0}$ is the SRH lifetime at BOL, K_{τ_α} is the minority carrier lifetime damage constant and ϕ is the 1-MeV electron fluence. The lifetime damage constant K_{τ_α} is expected to be material dependent and is fitted in the model within a range of values consistent with those reported in the literature.[27,47] In order to explain the observed changes in the spectral response and dark I-V upon irradiation, we had to postulate an increase of the surface recombination velocity at the window and BSF hetero-interfaces. This points out a degradation of the interface quality possibly due to radiation-induced defect states. The degradation of S_p and S_n is considered to be linearly dependent on the fluence and expressed by

$$S_\alpha = S_{\alpha(BOL)} + K_{S_\alpha}\phi, \tag{7}$$

where $S_{\alpha(BOL)}$ is the value of S_α at BOL and K_{S_α} is the interface damage rate, deduced from the best CPS model fit to the experimental data. The EQE, illuminated and dark $J-V$ measurements from the five studied structures are simultaneously taken in consideration in order to obtain a consistent fit value for K_{τ_α} and K_{S_α}.

The degradation mechanism of the J_{sc} of the solar cells under irradiation can be understood from the analysis of the measured EQE curves, shown in Figures 5 and 6 together with the simulated curves for different irradiation doses. Upon irradiation, the displacement damage creates defect states throughout the solar cell structure, which can act either as recombination centers for electron-hole pairs or as trap centers for electrons or holes. The former causes increased recombination rates, reducing the effective SRH lifetime and diffusion length of the minority carriers.[30-34] The latter, instead, perturbs the net charge profile across the sample, since trapping of majority carriers yields a local decrease of their density, the so-called carrier removal effect.[27] The decrease of the majority carrier density is directly proportional to the density of defects, and therefore, to the irradiation fluence, with a rate that for GaAs is on the order of 0.5 to 5 cm^{-1}.[27] In view of the moderate level of the maximum fluence and of the used doping levels in the cell structures, the effect is marginal in the present study. The difference in degradation behavior of the SJ and DJ cells is related to the fact that the transmission of light into the cell decreases exponentially, so that by far the largest fraction of light is absorbed at the upper part of the cell.

In the SJ cells, most of the photogenerated free carriers, therefore, only have to diffuse over a short distance to the pn-junction to be drifted towards the right electrode and be collected. This is particularly true for carriers generated by short wavelength light. For longer wavelengths a smaller fraction of the light is able to penetrate deeper into the cell and consequently generates some minority carriers deeper in the base, which have to travel further before reaching the pn-junction. Therefore, the short wavelength photocurrent is mostly sustained by the thin emitter, whereas most of the long wavelength photocurrent is supported by the thick base. Electrons generated deeper in

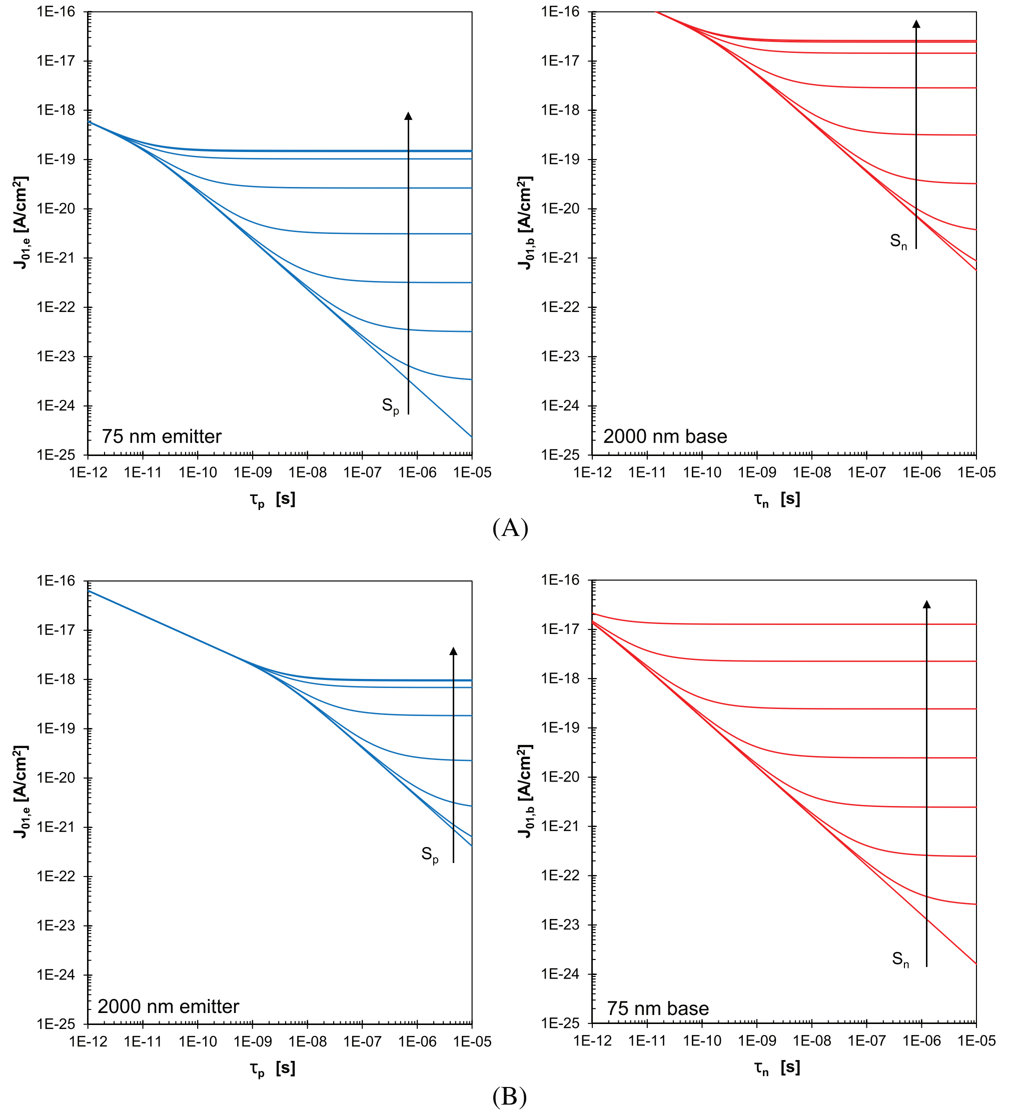

FIGURE 8 Analysis of the dependence of the saturation current density components in the emitter (left) and base (right) for A, a thin-film shallow junction cell and B, a thin-film deep junction cell as a function of minority carrier lifetime for different values of interface recombination velocities. S_p and S_n scale logarithmically from 10^0 to 10^7 cm/s in the direction of the arrow [Colour figure can be viewed at wileyonlinelibrary.com]

the thick base of SJ devices suffer more from the enhanced SRH recombination probability, as shown by the reduced EQE at longer wavelengths (see Figure 5). Based on the EQE analysis, the modeled degradation of τ_p and S_p is well correlated to the penalty observed in the short wavelength region, while the degradation of τ_n explains the penalty observed in the long wavelength region. Finally, the correlation between the simulations and measured EQE show that after irradiation there is a decrease in the contribution from the depletion region to the EQE, which might indicate a reduction of the depletion region thickness. This can be related, for example, to a strong change of the equilibrium carrier density in the base,[48] but a more detailed investigation to verify this assumption is required.

Differently from the SJ cells, in DJ cells all the minority carriers photogenerated in the emitter (except for the small fraction generated deeper in the cell) have to diffuse over a long distance before reaching the pn-junction. Therefore, the degradation of τ_p and S_p in the emitter reduces the collection efficiency over the entire wavelength range in the DJ cell (see Figure 6), resulting in a significant reduction of J_{sc}, whereas the impact of the base parameters is restricted to the longer wavelength region and turns out to be completely marginal. In fact, the significant asymmetry of the spectral response between the short and the long wavelength ranges observed for the DJ cells after irradiation can only be correctly modeled if an increased S_p is assumed, supporting the approach described in Equation (7).

In summary, the EQE upon irradiation is influenced mainly by the lifetime in the emitter for DJ cells and by the lifetime in both emitter and base for SJ cells. Moreover, the observed increase in S_p in both SJ and DJ cells upon irradiation indicates a degradation in the emitter-window hetero-interface quality.

The study of the dark $J-V$ characteristics upon irradiation (see Figure 7) provides further insight especially for the base parameters in the DJ cells. In fact, the observed increase of J_{01} in the DJ cells can only be explained by a significant increase of the recombination current component in the thin base. This in turn calls for an unusually high damage rate (K_{τ_n}), about two orders of magnitude higher than what is commonly reported in the literature.[27,47] Considering a more realistic value of K_{τ_n} (in the 10^{-6} cm^2/s range) implies that the base surface recombination velocity S_n has also a non-negligible value that increases with irradiation. For all the DJ configurations, the extracted J_{01} values could be explained by S_n values higher than 10^6 cm/s at EOL, suggesting a significant degradation at the base-BSF interface. Such a high S_n also implies that $J_{01,B}$ is dominated by S_n for cells with the DJ

TABLE 6 Values for the radiation induced damage rates deduced from the $J-V$ and EQE measurements of the cells

Solar Cell Geometry	Damage Rates			
	K_{τ_p} (cm²/s)	K_{τ_n} (cm²/s)	K_{S_p} (cm³/s)	K_{S_n} (cm³/s)
SB - SJ	8.75×10^{-7}	5.25×10^{-6}	1.7×10^{-11}	–
SB - DJ	1.75×10^{-6}	–	3.5×10^{-11}	1.3×10^{-8}
TF - SJ	8.75×10^{-7}	5.25×10^{-6}	3.4×10^{-11}	–
TF - DJ	8.75×10^{-7}	–	6.7×10^{-11}	4.6×10^{-9}
TF - DJ_{1400nm}	8.75×10^{-7}	–	4.6×10^{-11}	6.6×10^{-9}

geometry, as can be observed in Figure 8, and is quite insensitive to τ_n as long as the L_n/d_B ratio remains higher than one. Therefore, the electron lifetime cannot be reliably extracted.

In order to determine the damage rates, an approach was taken in which initially K_{τ_p} and K_{τ_n} were assumed to be the same for all configurations and then adjusted by closely fitting the model outcomes to the measured EQE, average illuminated $J-V$ parameters and dark $J-V$ curves. The fitted EOL values for τ_α, L_α and S_α resulting from this approach are depicted in the right portion of Table 4. Because the depletion region in the DJ solar cells is much closer to the base-BSF hetero-interface, the increase in S_n is the limiting mechanism to the performance for this geometry, rather than the decrease in τ_n, and the values for K_{τ_n} cannot be deduced. Therefore, the τ_n values shown in Table 4 for the DJ cell are set equal to those extracted from the analysis of the SJ cells. Conversely, in the SJ solar cells the junction distance to the rear interface is so large that the increase in S_n is hardly relevant to the performance, and therefore the values for K_{S_n} cannot be determined. The extracted values of K_{τ_p}, K_{τ_n}, K_{S_p} and K_{S_n} for the various cell geometries under study are stated in Table 6.

The hypothesis of a linear dependence of the recombination velocities with irradiation fluence provides a very good agreement between measured and simulated values of J_{sc}, V_{oc} and η for the whole fluence range, as seen from the detailed comparison of measured and simulated data in Figure 4 and in Table 3. Overall, the observed degradation of the performance of the solar cells upon irradiation is satisfactorily simulated assuming similar lifetime damage rates for electrons and holes for all the architectures of the solar cells, indicating that the material radiation damage is probably not affected by the device geometry or the fabrication steps. The identified values for the lifetime damage constant of minority electrons and holes are in good agreement with previous studies.[27,47] In particular, taking into account the carriers' diffusivity, the ratio K_{τ_n}/K_{τ_p} corresponds to a ratio in terms of diffusion length damage constant of about one tenth, inferring a damage rate for the diffusion length in n-type GaAs about ten times larger than that one in p-type GaAs, as theoretically predicted by Yamaguchi et al.[27]

The thickness of the active layers and the position of the depletion region are shown to be the determinant parameters with regards to the radiation resistance of the cells. Thin-film devices present the big advantage of having a back reflector that allows the thickness of the active layers to be significantly reduced. Therefore, a shallow junction solar cell processed into a thin-film geometry is found to be the best structure for space applications. The MOCVD growth of hetero-interfaces such as GaAs/AlInP and GaAs/InGaP has been shown to be a challenge in the past.[49-52] A meticulous control of chemical composition, material inter-diffusion and surface segregation is necessary in order to prevent the formation of mixed compounds that reduce the abruptness of the interfaces. The fact that interface recombination velocity is affected by irradiation indicates that it is an important aspect to be optimized, with the potential to further increase the resilience of the TF - SJ devices under irradiation.

4 | CONCLUSIONS

A combined experimental and theoretical analysis of the performance of GaAs solar cells upon electron radiation exposure is presented. In order to deduce the important cell parameters, five different solar cells architectures were applied, and the environment the cells would face in GEO and LEO space missions was simulated by subjecting the devices to electron fluences up to 1×10^{15} e⁻/cm².

The GaAs minority carriers' lifetime damage constants reported in the literature, required for a proper prediction of the cells performance in space application, differ significantly. In this study, by simultaneously analyzing the performance of the five different cells geometries, a coherent set of lifetime damage constants could be derived. The damage constants are found to be material dependent and insensitive to the device geometry or fabrication steps. The incidence of electrons introduces lattice defects in the cells that act as recombination centers, directly impacting carrier lifetimes. Because for the DJ cells at EOL the hole diffusion length is smaller than the emitter thickness, the collection of generated carriers is strongly reduced, and this geometry presents a much larger decrease of J_{sc} when compared to SJ devices. Therefore, we find that DJ cells in the present configuration are not suited for space application.

Most importantly, however, the modeling study has pointed out that besides the reduction of the lifetime of the carriers, the electron irradiation strongly affects the quality of hetero-interfaces, characterized by a linear increase in the interface recombination velocity. The current study shows that the degradation of the window-emitter and base-BSF hetero-interfaces quality is responsible for a significant increase of the diffusion component of the dark current, and consequently for the reduction of V_{oc}. Therefore, it is a critical aspect which deserves further investigation since it can become the bottleneck for the optimization of the cell radiation tolerance.

A shallow junction solar cell processed into a thin-film geometry is found to be the best structure for space applications, presenting an EOL average efficiency that is 82% of the BOL value. The presence of a rear reflector in the thin-film geometry allows the design of thinner devices that show the potential to further increase the BOL

performance and the resilience under irradiation, provided that the interface radiation hardness can also be improved.

ACKNOWLEDGEMENTS

The authors would like to thank the support from Marinus Hom of the RID during the performance of the irradiation tests and financial support from the Brazilian National Council for Scientific and Technological Development, under the program Science Without Border, project 233259/2014-7, and from the European Union's Horizon 2020 research and innovation program, under grant agreement 687253 TFQD (http://tfqd.eu).

ORCID

Natasha Gruginskie https://orcid.org/0000-0001-6571-0538
Federica Cappelluti https://orcid.org/0000-0003-4485-9055

REFERENCES

1. Green MA, Hishikawa Y, Dunlop ED, Levi DH, Hohl-Ebinger J, Ho-Baillie AW. Solar cell efficiency tables (version 51). *Prog Photovolt Res Appls*. 2018;26(1):3-12.
2. Feenstra J, Leest RHV, Smeenk NJ, et al. *Flexible shielding layers for solar cells in space applications*. vol. 28; 2016:43661.
3. Strobl GFX, Ebel L, Fuhrmann D, et al. Development of lightweight space solar cells with 30% efficiency at end-of-life. In: *2014 IEEE 40th Photovoltaic Specialist Conference (PVSC)*; 2014:3595-3600.
4. Colin C, Jaouad A, M Darnon C, et al., "The handling of thin substrates and its potential for new architectures in multi-junction solar cells technology," *AIP Conference Proceedings*, vol. 1881, no. 1, p. 040001, 2017.
5. Smeenk NJ , Mooney C, Feenstra J, et al. Space environmental testing of fl exible coverglass alternatives based on siloxanes. *Polym Degrad Stab*. 2013;98(12):2503-2511.
6. Kwak P, Kim N, Kim J, Kim D, Song K, Lee J. Flexible space solar cell array with radiation shield fabricated by guided-printing of cover glasses. *Solar Energy Materials and Solar Cells*. 2017;169, April:210-214.
7. Konagai M, Sugimoto M, Takahashi K. High efficiency GaAs thin film solar cells by peeled film technology. *J Cryst Growth*. 1978;45(C):277-280.
8. Yablonovitch E, Gmitter T, Harbison JP, Bhat R. Extreme selectivity in the lift-off of epitaxial GaAs films. *Appl Phys Lett*. 1987;51(26):2222-2224.
9. Voncken MMAJ, Schermer JJ, van Niftrik ATJ, et al. Etching AlAs with HF for epitaxial lift-off applications. *J Electrochem Soc*. 2004;151(5):G346–G351.
10. Voncken MMAJ, Schermer JJ, Bauhuis GJ, Mulder P, Larsen PK. Multiple release layer study of the intrinsic lateral etch rate of the epitaxial lift-off process. *Appl Phys A: Materials Sci Process*. 2004;79(7):1801-1807.
11. Tatavarti R, Hillier G, Dzankovic A, et al. Lightweight, low cost gaas solar cells on 4″ epitaxial liftoff (elo) wafers. In: *Proceedings 33rd IEEE Photovoltaic Specialists Conference*; 2008:1-4.
12. Bauhuis GJ, Mulder P, Haverkamp EJ, et al. Wafer reuse for repeated growth of III-V solar cells. *Prog Photovolt Res Appl*. 2010;18(3):155-159.
13. Stender CL , Adams J, Elarde V, et al, Flexible and lightweight epitaxial lift-off GaAs multi-junction solar cells for portable power and UAV applications, 2015 *IEEE 42nd Photovoltaic Specialist Conference, PVSC* 2015, pp. 8–11, 2015.
14. Hirst LC, Yakes MK, Warner JH, et al. Intrinsic radiation tolerance of ultra-thin GaAs solar cells. *Appl Phys Lett*. 2016; 109(3):033908-1, 033908-4.
15. Cappelluti F, Ghione G, Gioannini M, et al. Novel concepts for high-efficiency lightweight space solar cells. In: *E3S Web Conf*. Vol. 16; 2017:03007.
16. Bauhuis GJ, Schermer JJ, Mulder P, Voncken MMAJ, Larsen PK. Thin film GaAs solar cells with increased quantum efficiency due to light reflection. *Solar Energy Materials and Solar Cells*. 2004;83(1):81-90.
17. Kayes BM, Nie H, Twist R, et al. 27.6% Conversion efficiency, a new record for single-junction solar cells under 1 sun illumination. In: *Proceedings of the 37th IEEE Photovoltaic Specialists Conference*; 2011:04-08.
18. Miller OD, Yablonovitch E, Kurtz SR. Intense internal and external fluorescence as solar cell approach the SQ efficiency limit. *IEEE J Photovolt*. 2012;2(3):1-27.
19. Steiner MA, Geisz JF, García I, Friedman DJ, Duda A, Kurtz SR. Optical enhancement of the open-circuit voltage in high quality GaAs solar cells. *J Appl Phys*. 2013;113:123109-1, 123109-11.
20. Lumb MP, Steiner MA, Geisz JF, Walters RJ. Incorporating photon recycling into the analytical drift-diffusion model of high efficiency solar cells. *J Appl Phys*. 2014;116(19):194504, 1–10.
21. Gruginskie N, van Laar S, Bauhuis G, et al. *Increased performance of thin-film gaas solar cells by rear contact/mirror patterning*. *Thin Solid Films*; 2018.
22. Saravanan S, Krishna Teja T, Dubey RS, Kalainathan S. Design and analysis of GaAs thin film solar cell using an efficient light trapping bottom structure. *Mater Today Proc*. 2016;3(6):2463-2467.
23. Cappelluti F, Kim D, van Eerden M, et al. Light-trapping enhanced thin-film III-V quantum dot solar cells fabricated by epitaxial lift-off. *Solar Energy Mater Solar Cells*. 2018;181(2017):83-92.
24. Vagidov NZ, Montgomery KH, Bradshaw GK, Wilt DA. Light trapping structures for radiation hardness enhancement of space solar cells. *Solar Energy Mater Solar Cells*. 2018;182:136-141.
25. Bauhuis G, Mulder P, Hu YY, Schermer J. Deep junction III-V solar cells with enhanced performance. *Phys Status Solidi (A) Appl Mater Sci*. 2016;213(8):2216-2222.
26. Geisz JF, Steiner MA, García I, Kurtz SR, Friedman DJ. Enhanced external radiative efficiency for 20.8% single-junction GaInP solar cells. *Appl Phys Lett*. 2013;103:041118-1, 041118-5.
27. Yamaguchi M, Amano C. Numerical analysis for radiation-resistant GaAs heteroface solar cell structures. *J Appl Phys*. 1985;57(2):537-544.
28. Steiner MA, Lumb MP, Hoheisel R, et al. Radiation effects on luminescent coupling in III-V solar cells. In: *2015 IEEE 42nd Photovoltaic Specialist Conference (PVSC)*; 2015:1-5.
29. Van Leest R, Mulder P, Gruginskie N, et al. Temperature-induced degradation of thin-film III-V solar cells for space applications. *IEEE J Photovolt*. 2017;7(2):702–708.
30. Bourgoin JC, Zazoui M. Irradiation-induced degradation in solar cell: characterization of recombination centres. *Semicond Sci Technol*. 2002;17(5):453-460.
31. Warner JH, Messenger SR, Walters RJ, et al. Correlation of electron radiation induced-damage in GaAs solar cells. *IEEE Trans Nucl Sci*. 2006;53(4):1988-1994.
32. Salzberger M, Rutzinger M, Nömayr C, Lugli P, Zimmermann CG. Voltage-dependent photocurrent in irradiated GaAs solar cells. *Prog Photovolt Res Appl*. 2018;2017:1-7.
33. Pellegrino C, Zimmermann CG. Difference in space-charge recombination of proton and electron irradiated GaAs solar cells. *Prog Photovolt Res Appl*. 2019;27(2018):379-390.
34. Anspaugh BE. *GaAs Solar Cell Radiation Handbook*, 1996.

35. Schemer JJ, Mulder P, Bauhuis GJ, Larsen PK, Oomen G, Bongers E. Thin-film GaAs epitaxial lift-off solar cells for space applications. *Prog Photovolt Res Appl*. 2005;13(7):587-596.
36. Mazouz H, Logerais PO, Belghachi A, Riou O, Delaleux F, Durastanti JF. Effect of electron irradiation fluence on the output parameters of GaAs solar cell. *Int J Hydrogen Energy*. 2015;40(39):13857-13865.
37. Imaizumi M, Taylor SJ, Yamaguchi M, Ito T, Hisamatsu T, Matsuda S. Analysis of structure change of Si solar cells irradiated with high fluence electrons. *J Appl Phys*. 1999;85(3):1916-1920.
38. Wolf M, Rauschenbach H. Series resistance effects on solar cell measurements. *Adv Energy Convers*. 1963;3:455-479.
39. Hovel H. Semiconductors and semimetals. volume 11. solar cells, 1975.
40. Lumb MP, Bailey CG, Adams JGJ, et al. Extending the 1-D hovel model for coherent and incoherent back reflections in homojunction solar cells. *IEEE J Quantum Electron*. 2013;49(5):462-470.
41. Palik ED. *Handbook of optical constants of solids. Acdemic Press*, vol. 3, 1998.
42. Sotoodeh M, Khalid AH, Rezazadeh AA. Empirical low-field mobility model for III-V compounds applicable in device simulation codes. *J Appl Phys*. 2000;87(6):2890-2900.
43. Rein S. *Lifetime Spectroscopy: A Method of Defect Characterization in Silicon For Photovoltaic Applications*. Springer; 2005.
44. Tiwari S, Wright SL. Material properties of p-type gaas at large dopings. *Appl Phys Lett*. 1990;56(6):563-565.
45. Hudait MK, Modak P, Krupanidhi SB. Si incorporation and Burstein-Moss shift in n-type GaAs. *Mater Sci Eng B*. 1999;60(1):1-11.
46. Sah CT, Noyce RN, Shockley W. Carrier generation and recombination in p-n junctions. *Proc IRE*. 1957;45(9):1228–1243.
47. Bertness K, Cavicchi B, Kurtz S, Olson J, Kibbler A, Kramer C. Effect of base doping on radiation damage in GaAs single junction solar cells. *Conf Record Twenty-Second IEEE Photovolt Spc Conf*. 1991;2:1582-1587.
48. Hoheisel R, Gonzalez M, Lumb MP, et al. Quantum-well solar cells for space: the impact of carrier removal on end-of-life device performance. *IEEE J Photovolt*. 2014;4(1):253-259.
49. Nakano T, Shioda T, Enomoto N, et al. Precise structure control of GaAs/InGaP hetero-interfaces using metal organic vapor phase epitaxy and its abruptness analyzed by STEM. *J Cryst Growth*. 2012;347(1):25-30.
50. Fukushima Y, Nakano T, Nakano Y, Shimogaki Y. Control of in surface segregation and inter-diffusion in GaAs on InGaP grown by metal-organic vapor phase epitaxy. *Jpn J Appl Phys*. 2012;51:055601-1, 055601-5.
51. Wells NP, Driskell TU, Hudson AI, et al. Carrier quenching in InGaP/GaAs double heterostructures. *J Appl Phys*. 2015;118:065703-1, 065703-10.
52. López-escalante MC, Gabás M, García I, Barrigón E, Rey-stolle I, Algora C. Applied Surface Science Differences between GaAs/GaInP and GaAs/AlInP interfaces grown by movpe revealed by depth profiling and angle-resolved X-ray photoelectron spectroscopies. *Appl Surf Sci*. 2016;360:477-484.

How to cite this article: Gruginskie N, Cappelluti F, Bauhuis GJ, et al. Electron radiation–induced degradation of GaAs solar cells with different architectures. *Prog Photovolt Res Appl*. 2020;1–13. https://doi.org/10.1002/pip.3224